THE ASTROPHYSICAL JOURNAL, 518:183–189, 1999 June 10

A SUPER–STAR CLUSTER IN NGC 253: MID-INFRARED PROPERTIES

ERIC KETO, JOSEPH L. HORA, AND G. G. FAZIO
Smithsonian Astrophysical Observatory, 60 Garden Street, Cambridge, MA 02138
WILLIAM HOFFMANN
Steward Observatory, University of Arizona, Tucson, AZ 85721
AND
LYNNE DEUTSCH
Astronomy Department, Boston University, 725 Commonwealth Avenue, Boston, MA 02215
Received 1998 February 26; accepted 1999 January 12

ABSTRACT

We observed the nearby starburst galaxy NGC 253 in the mid-infrared to obtain a three-dimensional data set with arcsecond angular resolution and 0.2 μm spectral resolution. The observations show the major spectral features in the upper half of the mid-IR window: the 11.3 μm polycyclic aromatic hydrocarbon (PAH) line and the 12.8 μm [Ne II] line as well as the broad silicate absorption feature at 9.7 μm. We use the [Ne II] line to determine the emission measure of the ionized gas, and in combination with radio observations to predict the thermal and nonthermal contributions to the radio continuum. The amount of ionized gas is related to the rate of star formation. Based on the mid-IR spectra, we identify three major components in the nucleus of NGC 243: an AGN in the center of the galaxy, a super–star cluster also seen in optical images, and a larger scale diffuse envelope composed of an older population of supernova remnants and lower mass stars.

Subject headings: galaxies: individual (NGC 253) — galaxies: starburst — galaxies: star clusters

1. INTRODUCTION

The galaxy NGC 253 is a nearby ($\sim$3 Mpc) Sb/Sc spiral with an active starburst nucleus. Previous near and mid-IR imaging and spectroscopy suggest several components in the starburst nucleus (Rieke & Low 1975; Wynn-Williams et al. 1979; Rieke et al. 1980; Beck & Beckwith 1984; Lebofsky, Montgomery, & Kailey 1985; Scoville et al. 1985; Turner & Ho 1985; Antonucci & Ulvestad 1988; Rieke, Lebofsky, & Walker 1988; Ho et al. 1989; Ho, Beck, & Turner 1990; Forbes, Ward, & DePoy 1991; Roche et al. 1991; Ulvestad & Antonucci 1991, 1994, 1997; Pina et al. 1992; Keto et al. 1993; Carral et al. 1994; Sams et al. 1994; Kalas & Wynn-Williams 1994). Most of the emission derives from an extended envelope, of about 100 pc scale, which defines the extent of the IR nucleus, but a significant fraction of the IR power is contained in two bright peaks separated by 3″. The weaker of these peaks is identified with the center of the galaxy, based on a coincidence in position with a bright nonthermal radio point source (Turner & Ho 1985). The brighter IR peak does not have an obvious radio counterpart, and its nature has been enigmatic. More recent observations with the *Hubble Space Telescope* (*HST*) have identified a bright optical star cluster at the position of this IR peak (Watson et al. 1996). In the optical, the star cluster appears similar in size and brightness to the super–star clusters seen by the *HST* in a wide range of starburst environments (Holtsmann et al. 1992; Benedict et al. 1993; Whitmore et al. 1993; Conti & Vacca 1994; Shaya et al. 1994; Barth et al. 1995; Bower & Wilson 1995; Whitmore & Schweizer 1995; Meurer et al. 1995).

We observed NGC 253 with a mid-IR camera in order to measure the 12.8 μm [Ne II] line. The [Ne II] line is useful because it is directly related to the emission measure of the ionized gas, which in turn can be used to estimate various quantities such as the number of ionizing photons and the number of massive stars. This paper reports our observations and derives some quantities useful for understanding the starburst in NGC 253.

2. OBSERVATIONS AND DATA ANALYSIS

We observed the nucleus of NGC 253 with the mid-infrared imaging camera MIRAC2 (Hoffman et al. 1993, 1998) mounted on the 3 m telescope at the Infrared Telescope Facility (IRTF),[1] on 1995 December 8 and 9. We used a circular variable filter (CVF) with a spectral resolution of about 2% to make a sequence of 24 images separated in wavelength by about 0.2 μm across the mid-IR window. Combined, these images give us a spectrum at each spatial pixel with a spectral resolution sufficient to identify the major features in the mid-IR window: the 8.6 μm polycyclic aromatic hydrocarbon (PAH) line, the 9.7 μm silicate absorption feature, the 11.2 μm, PAH feature, and the 12.8 μm [Ne II] line. The angular resolution was seeing limited at about 1″ with a plate scale of 0.31×0.31 arcsec^2 pixel^{-1}. We used one-quarter of the 128×128 pixel array for each of 4 beam positions in a square nod-chop pattern resulting in a $20'' \times 20''$ field of view. The observations are calibrated for absolute flux and position.

Observations with the CVF were made at the following wavelengths: 7.68, 7.79, 8.01, 8.24, 8.35, 8.60, 8.86, 9.00, 9.14, 9.27, 10.86, 11.04, 11.23, 11.42, 11.62, 11.81, 12.01, 12.21, 12.41, 12.61, 12.81, 13.01, 13.21, and 13.42 μm. The filter has a triangular bandpass with a spectral resolution of about 0.102 μm FWHM at the short-wavelength end of the mid-IR window and a resolution of 0.215 μm at the long-wavelength end. We used discrete wavelength filters with a 10% bandpass in the center of the mid-IR window, 9.8 and

[1] The NASA Infrared Telescope Facility is operated by the University of Hawaii under contract with the National Aeronautics and Space Administration.

10.3 μm, where the emission is relatively weak, because the wider bandpass provides for a better signal-to-noise ratio. The data between 7.6 and 13.4 μm were interpolated to a uniform bandwidth of 0.2 μm. Additionally we observed the galaxy at 20.2 μm with 10% resolution.

The images were calibrated by comparison with the spectra of standard stars published by Cohen et al. (1995). The images have been corrected for flat field and bad pixels by standard techniques (Hoffmann & Hora 1997). We remove the effect of atmospheric absorption by first fitting for the atmospheric extinction, and second by correcting for the extinction. The fitting is possible because the atmospheric transmission varies with wavelength, and therefore the shape of the spectra in our measurements of the standard stars depends on the extinction. Comparison of the measured shapes with the expected shapes above the atmosphere (Cohen et al. 1995) for our calibrator stars β And and β Peg gave optical depths of 1.40 and 1.35 times the zenith optical depth of the model atmosphere (Cohen et al. 1995), implying an uncertainty of 5%, At each wavelength, we use this optical depth and the atmospheric model to correct the counts of our standard stars and the galaxy to above the atmosphere. Once above the atmosphere, we can smooth the channel-to-channel noise in our measurements of the calibrator stars to improve the signal-to-noise ratio. We then calibrate each of our galaxy images at the different wavelengths separately, taking into account the transmission function of the filter used. The rms noise in each image provides an estimate of the relative uncertainty within the image: about 30 mJy arcsec^{-2} for the longer wavelengths and 100 mJy arcsec^{-2} for the wavelengths less than 9 μm. The difference in the noise levels is due to changing weather conditions.

Our data show a total 12.4 μm flux of 20 Jy within a 0.2 μm bandpass, almost twice the flux density from our previous observation made at 12.5 μm with a bandpass filter of 1.25 μm (Keto et al. 1993). The different bandpasses coupled with the feature-rich mid-IR spectrum will account for some of the difference. But our previous experience with mid-IR calibration suggests that a more significant source of uncertainty is in the strengths of the calibrator stars, particularly when viewed with the different bandpasses used by different instruments. Use of the new calibration spectra of Cohen et al. (1995) should help improve mid-IR calibration because these standard spectra can be convolved with any instrumental filter function to derive appropriate calibrator fluxes for a particular instrument.

The brightest mid-IR peak was assigned the position that we had previously measured for this feature by offsetting to nearby stars (Keto et al. 1993). The position of this peak has also been measured in the near-IR (Kalas & Wynn-Williams 1994). Based on these previous measurements, the absolute positional accuracy (3 σ) is about an arcsecond.

Figures 1–4 show the images of NGC 253 in the off-line bands around 12.8 μm, the [Ne II] line at 12.8 μm, the 11.3 μm PAH line, and the 20.2 μm continuum. The 12.8 μm off-line image (Fig. 1) is the average of the filter bands at 12.4 and 13.2 μm which are on either side of the [Ne II] line. The difference of the band at 12.8 μm and the averaged off-line bands is the [Ne II] image (Fig. 2). Although the off-line band measures the emission on either side of the [Ne II] line, the level of the dust continuum is uncertain because of PAH emission across the mid-IR window. A recent *ISO* spectrum shows that in at least one galaxy, Circinus, there is

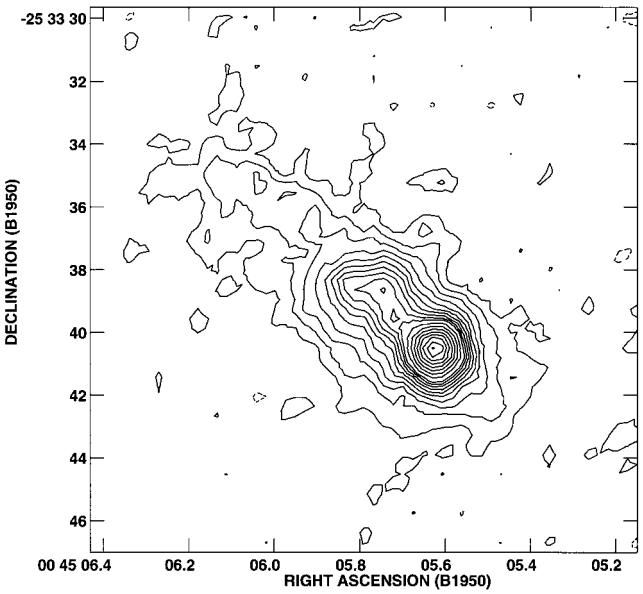

FIG. 1.—Average of the emission from the filter bands at 12.4 and 13.2 μm. This approximates the off-line or continuum emission at 12.8 μm, the location of the [Ne II] line. The lowest 10 contour levels are in steps of 0.075 and 0.15 Jy arcsec^{-1} thereafter.

a broad feature of enhanced emission longward of the deep silicate absorption feature (Moorwood et al. 1996). If a similar feature is present in NGC 253, then because this feature is so flat and much broader than the 12.8 μm [Ne II] line, subtracting the off-line bands from the band at 12.8 μm will still yield the [Ne II] line emission. The contribution of PAH emission to the on-line band is also uncertain. For example, our spectral resolution does not allow us to separate the 12.7 μm PAH feature from the 12.8 μm [Ne II] line. There might be some contribution from this PAH feature in our [Ne II] image.

We can identify three spectrally distinct components in the nucleus: the two small, bright sources and the surround-

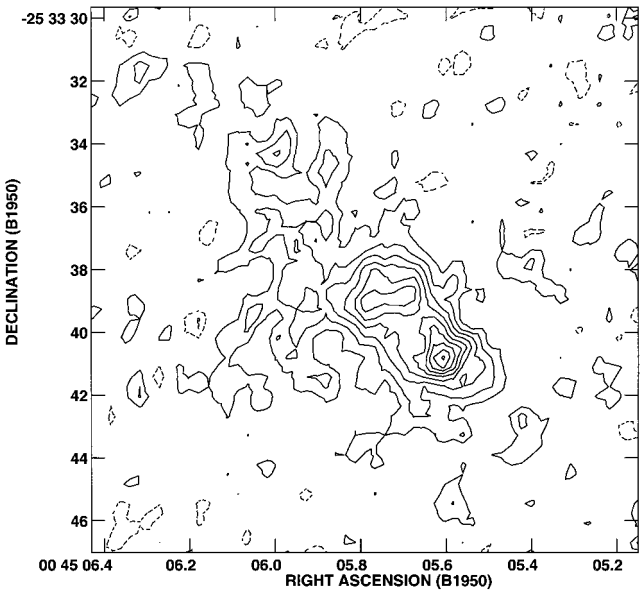

FIG. 2.—[Ne II] line emission at 12.8 μm. This image is formed from the difference of the emission in the 12.8 μm filter band and the off-line emission in Fig. 1. The contour levels are in steps of 0.075 Jy arcsec^{-1}. Dashed lines indicate negative contours.

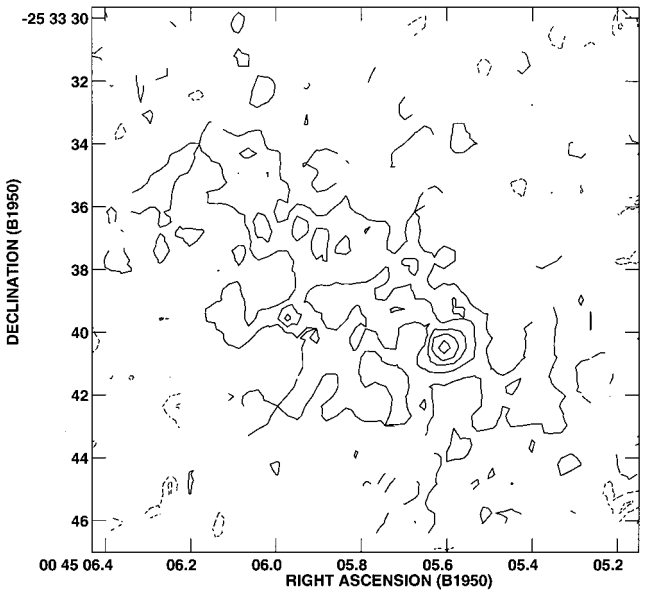

FIG. 3.—PAH emission at 11.3 μm. This image is formed by averaging the bands at 11.2 and 11.4 μm and subtracting the average of the bands at 11.0 and 11.6 μm. The contour levels are in steps of 0.075 Jy arcsec^{-1}. Dashed lines indicate negative contours.

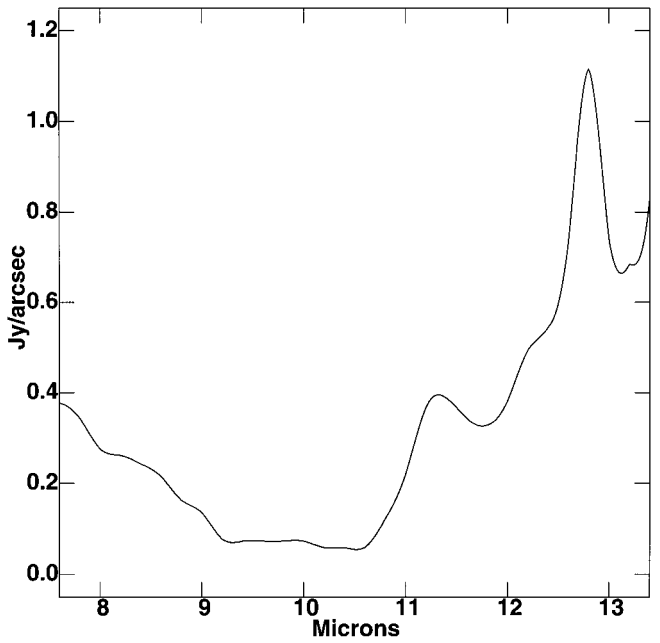

FIG. 5.—Spectrum at R.A.(1950) = 00^{h}45^{m}5^s.81, decl.(1950) = −25°33′38″.8, the position of the center of the galaxy. Note the PAH emission feature at 11.3 μm and the [Ne II] line at 12.8 μm.

ing envelope of lower level emission. Figures 5–7 show spectra from single pixels at the position of the center of the galaxy [R.A.(1950) = 00^{h}45^{m}5^s.81, decl.(1950) = −25°33′38″.8] and the star cluster [R.A.(1950) = 00^{h}45^{m}5^s.63, decl.(1950) = −25°33′40″.5], and a spectrum from the envelope at a position east of the star cluster and south of the center of the galaxy [R.A.(1950) = 00^{h}45^{m}5^s.74, decl.(1950) = −25°33′40″.6]. Based on their coincidence in position, the brightest IR source to the southeast is the super–star cluster identified in the optical (Watson et al. 1996). The fainter IR source to the northwest is the center of the galaxy identified by its extreme nonthermal radio emission (Turner & Ho 1985; Ulvestad & Antonucci 1997). The third component is the larger scale envelope. The spectra show the [Ne II] line at 12.8 μm, the 11.3 μm PAH feature, and the 8.6 μm PAH feature. Because the quality of the data below 9 μm is poorer, about 100 mJy arcsec^{-2} versus 30 mJy arcsec^{-2} at 12 μm, we do not use the 8.6 μm feature in our analysis. The spectra and the images show that the ratios [Ne II]/continuum and 11.3 μm PAH/continuum are different in each of the three components, suggesting that these different regions have different IR properties, that is, different mixtures of molecular, atomic, and ionized gas and dust. Since the state of the gas depends on the quantity and

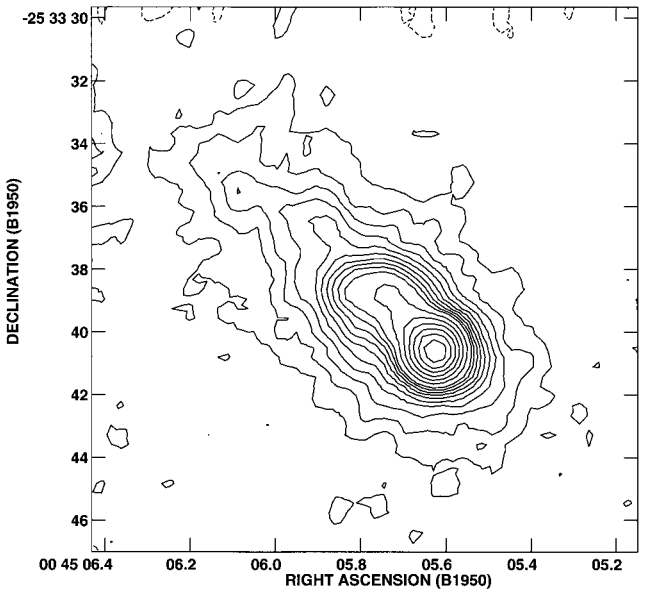

FIG. 4.—Emission at 20.2 μm. The lowest 10 contour levels are in steps of 0.14 Jy arcsec^{-1} and 0.28 Jy arcsec^{-1} thereafter.

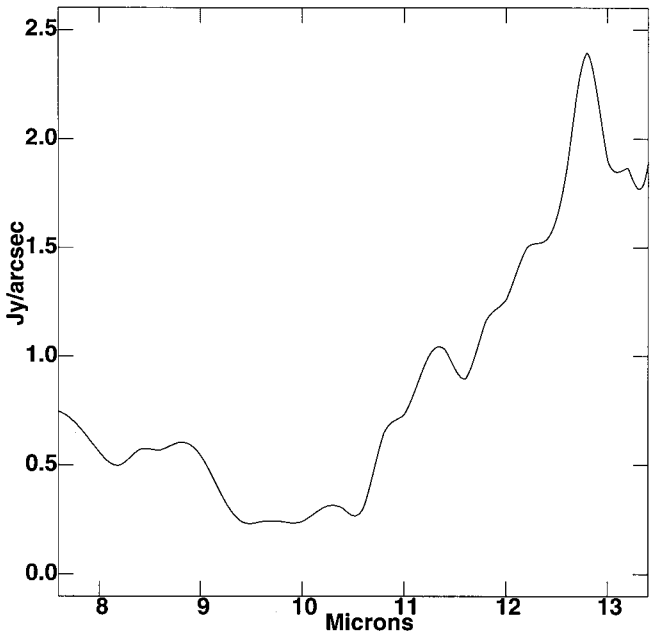

FIG. 6.—Spectrum at R.A.(1950) = 00^{h}45^{m}5^s.63, decl.(1950) = −25°33′40″.5, the position of the star cluster. Note the PAH emission feature at 11.3 μm and the [Ne II] line at 12.8 μm.

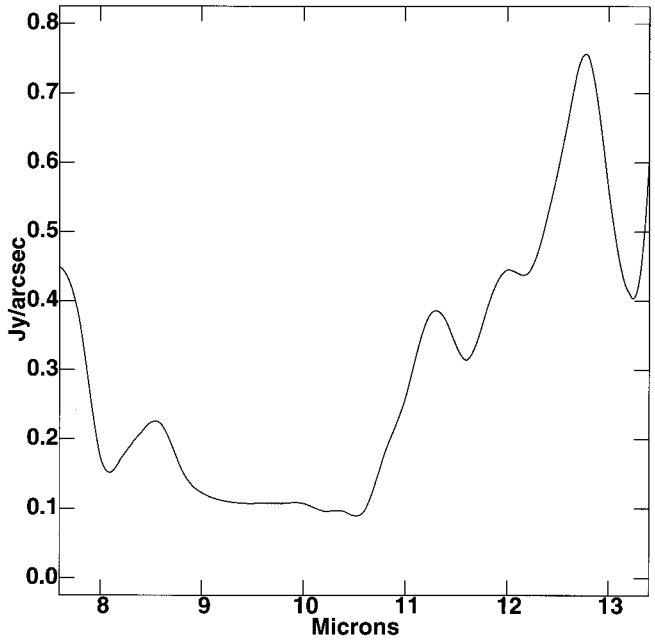

FIG. 7.—Spectrum at R.A.(1950) = $00^h45^m5\overset{s}{.}74$, decl.(1950) = $-25°33'40\overset{''}{.}6$, a position in the envelope west of the star cluster and south of the center of the galaxy. Note the PAH emission feature at 8.6 and 11.3 μm and the [Ne II] line at 12.8 μm.

hardness of the radiation heating it, these regions quite probably have different underlying power sources.

From the three images one can pick out other sources. For example, in the [Ne II] image (Fig. 2), the radio point source which marks the exact center of the galaxy is at the east (left) end of the small east-west bar of emission north of the star cluster. Either the emission associated with the center of the galaxy is extended, or there is another source to the west of the center of the galaxy between the center and the star cluster. The latter possibility is suggested because the western (right) end of the small bar becomes progressively brighter at longer wavelengths while the eastern (left) end fades. This results in the apparent wavelength-dependent position for this feature (Kalas & Wynn-Williams 1994). Nonetheless, in this paper we will analyze the three easily distinguished sources.

Table 1 gives the positions, sizes, and fluxes of the three components. The fluxes for the three components are derived by fitting three Gaussians simultaneously to an image of the spectral feature. At any position there is a sum of IR emission from the three different components. So, for example, in Table 1, the 12.8 μm continuum emission from the center of the galaxy is quite weak because most of the emission at that position is assigned to the underlying envelope component. However, the 12.8 μm [Ne II] line at the center of the galaxy is best fitted by a narrower component, implying little [Ne II] contribution from the envelope.

We estimate the upper limit of the optical depth at 9.8 μm as $\tau = -\ln\ (S_{9.8\ \mu\mathrm{m\ measured}}/S_{9.8\ \mu\mathrm{m\ continuum}})$. We derive the 9.8 μm continuum by measuring the slope of the emission between 20.2 and 12.8 μm and extrapolating to 9.8 μm. The reason we do not use our measurements around 8 μm to determine the slope is that this region of the mid-IR spectrum is known to be significantly influenced by the 8.6 and 7.7 μm PAH features. Our estimate of the optical depth is an upper limit because there may also be PAH emission in the 12.8 and 20.2 μm bands. For example, in an extreme case, the silicate absorption feature would be negligible if the measured 9.8 μm emission indicates the continuum level and the increased emission at 12.8 μm is due solely to PAH emission (Dudley & Wynn-Williams 1993, 1997).

3. DERIVED QUANTITIES

The [Ne II] line emission is directly related to the emission measure, $n_e^2\, l$, of the ionized gas, which in turn can be used to predict a number of quantities including the thermal radio continuum emission, the number of ionizing photons required to maintain the ionization, the number of O stars required to produce the ionizing photons, and the mid-IR continuum expected from the ionizing photons.

The [Ne II] fine-structure line at 12.8 μm is a two-level system between the $^2P_{3/2}$ and the $^2P_{1/2}$ states. The intensity depends on the number of atoms in the upper state,

$$I = \frac{h\nu A_{21}}{4\pi} \int n_e\, dl\ , \tag{1}$$

or (Petrosian 1970; Lacy, Beck, & Geballe 1982),

$$I(\mathrm{ergs\ s^{-1}\ cm^{-2}\ sr^{-1}}) = 3 \times 10^8 \left(\frac{10^4\ \mathrm{K}}{T_e}\right)^{1/2} \times e^{-h\nu/kT_e} \int \frac{n_c}{n_e + n_c} \times \gamma_{\mathrm{Ne}}\, n_e^2\, dl\ (\mathrm{cm^{-6}\ pc})\ , \tag{2}$$

where T_e, n_e, and n_c are the electron temperature, the density, and the critical density of [Ne II]. The number abundance of Ne relative to H is γ_{Ne}, with $\gamma_{\mathrm{H}^+} = 10^4$. We use $T_e = 10^4$, $\gamma_{\mathrm{Ne}} = 0.83$, $n_c = 3.6 \times 10^5$. We use the measured width of the [Ne II] line, which at our low resolution

TABLE 1

MEASURED QUANTITIES

Component	R.A.[a] (1950)	Decl. (1950)	Size[b] (arcsec^2)	$\tau_{9.8\ \mu\mathrm{m}}$[c]	11.3 PAH (Jy)	12.8 Continuum (Jy)	12.8 Ne II (Jy)	12.8 Continuum (Jy)
Star cluster.....	00 45 05.63	−25 33 40.5	1.5 × 1.5	0.8 (0.06)	0.18 (0.02)	4.3 (0.02)	1.8 (0.02)	10.8 (0.04)
Center	00 45 05.75	−25 33 38.8	2.4 × 2.0	0.3 (0.05)	<0.02 (0.02)	3.0 (0.01)	2.0 (0.02)	6.3 (0.03)
Envelope	00 45 05.78	−25 33 38.8	11.6 × 3.9	0.6 (0.01)	4.9 (0.01)	12.6 (0.01)	11.5 (0.01)	35.9 (0.01)

NOTE—Units of right ascension are hours, minutes, and seconds; units of declination are degrees, arcminutes, and arcseconds.

[a] Position uncertainties are $0\overset{''}{.}5$.

[b] Size uncertainties are $0\overset{''}{.}3$. Sizes were measured in the 12.8 μm continuum.

[c] $\tau = -\ln$ (9.8 μm/12.8 μm continuum); 1 σ uncertainties follow in parentheses. The uncertainty is based on the noise in the maps. However, the absolute flux calibration may have a 3 σ error of 25%.

was a little broader, 0.25 μm, than the CVF bandpass of 0.2 μm. We assume that the electron density is low enough that $n_c/(n_e + n_c) \sim 1$, and we assume that the [Ne II] line is optically thin. Table 2 shows the emission measure for our three selected components in NGC 253. With these assumptions,

$$n_e^2\, l(\mathrm{pc\ cm^{-6}}) = 7.0 \times 10^6 I_{\mathrm{Ne\ II}}(\mathrm{Jy\ arcsec^{-2}}) \times (\Delta\lambda_{\mathrm{FWHM}}/0.25\ \mu\mathrm{m})\ . \quad (3)$$

The [Ne II] optical depth can be estimated from the intensity by substituting with appropriate constants B_{12} for A_{21} and for n_2, n_1 times the ratio of the transition rates, downward over upward. Assuming an electron density of 1000 cm^{-3}, the optical depth in the [Ne II] line is much less than unity, about 0.001 for all three components. Because the upward collision rate varies linearly with density, the optical depth, for a given brightness, varies inversely with the unknown electron density. That is, if we assumed a lower electron density, say 100 cm^{-3}, the optical depth would be a factor of 10 higher—still much less than unity. This low optical depth implies that the [Ne II] line is not affected by self-absorption.

The emission measure is directly related to the thermal radio continuum. At 5 GHz the optical depth in the free-free continuum (Mezger & Henderson 1967),

$$\tau_{\mathrm{ff}} = 8.2 \times 10^{-2}\left(\frac{T_e}{\mathrm{K}}\right)^{-1.35}\left(\frac{\nu}{\mathrm{GHz}}\right)^{-2.1}\left(\frac{n_e^2\, l}{\mathrm{cm^{-6}\ pc}}\right), \quad (4)$$

is less than 0.001 at all positions if the temperature of the ionized gas, T_e, is 10^4 and less than 0.02 for $T_e = 5000$. Using the optically thin approximation, the brightness temperature $T_b = T_e\,\tau_{\mathrm{ff}}$, or, in flux units, $S_{5\ \mathrm{GHz}}(\mathrm{Jy}) = 1.6 \times 10^{-2} S_{[\mathrm{Ne\ II}]}(\mathrm{Jy})$. The predicted 5 GHz radio continuum, assuming $T_e = 10^4$, for our three components is presented in Table 2.

Using the thermal free-free radio continuum predicted by the [Ne II] observations, we can derive the nonthermal synchrotron radio emission as the difference between the observed or total radio continuum and the predicted free-free continuum. We compare the [Ne II] emission at the position of each of our three sources to the 5 GHz radio emission from Ulvestad & Antonucci (1997). We use the [Ne II] emission directly from Figure 2 rather than from the Gaussian components of Table 1 because the total [Ne II] emission at any point (Fig. 2) is a sum of fractions of the three Gaussians corresponding to their peaks and distances from the point. The radio flux of the source at the center of the galaxy may be taken as given by Ulvestad & Antonucci (1997). However, because the star cluster does not have an obvious radio counterpart (Pina et al. 1992; Keto et al. 1993; Kalas & Wynn-Williams 1994), we used the flux of the nearest radio point source, which is named 5.62 − 41.3 (Ulvestad & Antonucci 1997), as an upper limit, although this radio source may or may not be associated with the star cluster. The results are presented in Table 2. In the center of the galaxy, the nonthermal radio source dominates and the thermal emission is only 17% of the radio emission. In contrast, the radio emission from the star-forming supercluster is nearly all thermal, indicating a significant contribution from H II regions. Comparing the radio and [Ne II] in the larger scale envelope, we find the thermal emission is 30%–40% of the total radio.

From the emission measure, $n_e^2\, l$, derived from the [Ne II] observations, we can compute the number of ionizing photons, N_{UV}, necessary to maintain the ionization (Spitzer 1978, eq. [5-21]):

$$N_{\mathrm{UV}}(\mathrm{s^{-1}}) = n_e{}^2 l A \alpha^{(2)} = 1.28 \times 10^{52} S_{\mathrm{Ne\ II}}(\mathrm{Jy})\ , \quad (5)$$

where A is the area and $\alpha^{(2)}$ is the effective recombination coefficient for hydrogen to all levels except $n = 1$. The results are presented in Table 3. This calculation assumes that all the ionizing photons ionize the gas—in other words, no dust absorption. In principle, knowing the gas density and the gas-to-dust ratio, one can correct for the dust absorption (Petrosian, Silk, & Field 1972). For a gas density of about 1000 and a proton-to-dust ratio of 3000, the correction is about a factor of 4. The rate of ionizing photons implies a certain number of massive stars. One should properly consider the effects of the initial mass function (IMF), but as a first approximation, divide the total rate by that produced by a star of spectral type O6–O7, which is 10^{49} UV photons s^{-1}. The supercluster should therefore contain

TABLE 2

DERIVED QUANTITIES: RADIO

Component	$n_e^2 L$ (cm^{-6} pc)	Ne II[a] (Jy)	5 GHz Predicted (Jy)	5 GHz Measured (Jy)	Percent Thermal
Star cluster.....	3.5×10^6	0.6	9.7	$\lesssim$10.5	$\gtrsim$90
Center	2.8×10^6	0.5	7.4	44.2	17
Envelope	9.1×10^5	0.2	2.6	6.9	30–40

[a] Includes contribution from envelope component at positions listed in Table 1.

TABLE 3

DERIVED QUANTITIES: IONIZING PHOTONS AND IR

Component	N_{ionizing} (s^{-1})	$S_{12.8\ \mu\mathrm{m\ continuum}}$ Predicted (Jy)	$S_{12.8\ \mu\mathrm{m\ continuum}}$ Measured (Jy)	Ratio Measured/Thermal
Star cluster.....	4.0×10^{52}	1.5	4.3	3.0
Center	3.3×10^{52}	1.6	3.0	1.9
Envelope	1.6×10^{53}	7.3	12.6	1.7

on the order of a few times 10^3 or possibly as many as 10^4 O stars.

Assuming that all the ionizing photons are eventually degraded into the IR, one can compute the total expected IR emission and, assuming a gas temperature, the expected mid-IR continuum emission. The total energy flux due to ionizing photons ($h\nu_{\rm UV} = 13.6$ eV) is

$$S_{\rm tot} = \frac{h\nu_{\rm UV} N_{\rm UV}}{4\pi R^2}, \quad (6)$$

where R is the distance to the galaxy, about 3 Mpc. If the IR spectrum is given by the Planck function modified by the dust emissivity, ν^β, the fraction of the IR emerging at any wavelength is (Genzel et al. 1982; Ho, Beck, & Turner 1990)

$$S_\nu({\rm W\ m^{-2}\ Hz^{-1}}) = A_\beta \left(\frac{h\nu}{kT_e}\right)^{4+\beta} \frac{e^{\lambda/c} S_{\rm tot}}{e^{h\nu/kT_e} - 1}. \quad (7)$$

If $\beta = 1$, then $A_\beta = 4.02 \times 10^{-2}$. We can calculate an upper limit to the mid-IR emission by assuming a temperature of 300 K. Comparing this upper limit to the measured mid-IR emission (Table 3) suggests that the measured IR emission exceeds that predicted from the ionizing photons by a factor of a few. This difference could be accounted for by the presence of dust inside the H II regions which would increase the required UV photon rate by a factor of a few. However, assuming a gas temperature of 100 K rather than 300 K results in predicted mid-IR fluxes a factor of 8 lower, and a temperature of 25 K will produce no detectable mid-IR. We may conclude that the gas must be quite warm or that sources of energy other than ionizing photons are significant in heating the dust.

4. PROPERTIES OF THE NUCLEAR COMPONENTS

4.1. *The Super–Star Cluster*

If there are several super–star clusters (SSCs) visible in the *HST* optical images (Watson et al. 1996) why is one of the super–star clusters so singularly bright in the mifd-IR? The predominance of thermal radio emission from the cluster suggests that the cluster might be exceptionally young, less than 10^6 yr, and most of the O stars may still be on the main sequence. The fraction of nonthermal radiation should increase as the cluster ages and the O stars become supernovae, and, in addition, the supernovae may drive some of the gas and dust out of the cluster, reducing its mid-IR emission. The other clusters in the envelope may be in this more advanced stage.

Although the cluster may be very young, our observations suggest that the radiation of the star cluster is not dominated by ionizing radiation. This is inferred from the comparison of the power in the observed mid-IR continuum radiation and the power in the ionizing photons as deduced from the [Ne II] flux. There is more mid-IR radiation than could be produced from the down-conversion of the ionizing photons. This "mid-IR excess" has been noted in previous observations of the nuclei of several nearby starbursts including NGC 253 (Ho et al. 1989; Mouri et al. 1997). One interpretation of this mid-IR excess is that there is significant nonionizing radiation in the star cluster, which could be provided, for example, by supernova remnants or low-mass stars. Ho et al. (1989) suggested that low-mass stars could not provide the power for the mid-IR, by the following reasonable argument. Significant mid-IR radiation is only emitted by dust which has a temperature of 150 K or more. Such hot dust is found only within 0.1 pc of a typical OB star and within a closer distance around any later type. Because their observations, at lower angular resolution, appeared to show the mid-IR extended over several hundred parsecs, they reasoned that later type stars could not heat the diffuse gas in such a large volume to the required temperature. However, the recent *HST* observations mentioned in § 1 suggest that the star formation occurs in compact clusters, and it is the clusters that are distributed over several hundred parsecs. In this case the gas and stars are much more densely packed in the small volume of each of the clusters, and it might be possible for low-mass stars to heat the gas enough to produce significant mid-IR radiation. It has been suggested that the IMFs of starbursts are biased toward high-mass stars and that there are fewer low-mass stars than in the IMF of the solar neighborhood (Rieke et al. 1980, 1993). However, if the super star clusters are young globulars as suggested by Ho (1996) and Ho & Filippenko (1996a, 1996b), then the SSCs must be rich with low-mass stars (Paresce et al. 1995), which may produce most of the nonionizing radiation.

4.2. *The Center of the Galaxy*

The compact, nonthermal radio emission with its high brightness temperature indicates an AGN at the center of NGC 253. The 11.3 μm PAH feature suggests a significant difference in the properties of the gas around the AGN and in the super–star cluster. In contrast to the generous level of 11.3 μm PAH emission from the star cluster, the PAH emission from the bright, nonthermal radio source at the center of NGC 253 is relatively weak compared to the thermal emission indicated by the [Ne II] line (Figs. 3 and 2, respectively). In our Galaxy, PAH molecules are most often associated with photodissociation regions of molecular clouds which are found around the H II regions of massive stars and planetary nebulae (e.g., Cohen et al. 1989). The lower level of PAH emission in the center of the galaxy could be interpreted as indicating a higher ratio of ionized gas to photodissociated or molecular gas. It has been proposed that the hard spectrum of an AGN may destroy PAH molecules (Puget & Leger 1989; Roche et al. 1991). This proposal was made in a larger scale context based on lower angular resolution observations of the central several hundred parsecs of active galaxies with much more powerful AGNs than would be in NGC 253. Nonetheless, the relative lack of PAH emission in the central few parsecs of NGC 253 may be due to the hard spectrum of the mild AGN responsible for the nonthermal radio point source. Alternatively, perhaps it is not a question of the hardness of the radiation but one of the lack of dissociated molecular material. Observations of molecular emission (Paglione, Tosaki, & Jackson 1995; Peng et al. 1996) suggest plenty of molecular gas, but perhaps little of it is dissociated. For example, one ionizing source, the AGN, can dissociate a single shell of optical depth unity, whereas a large number of ionizing sources—for example, the O stars in a cluster—can potentially dissociate a much larger volume if they are distributed throughout the molecular gas each with its own dissociated shell of optical depth unity.

4.3. *The envelope*

Although the star cluster produces the brightest mid-IR emission, the larger scale envelope component contributes more to the total mid-IR and more to the "mid-IR excess"

of the galaxy (Tables 1 and 3). Following the discussion above, the mid-IR excess in the envelope may derive from a rich population of low-mass stars concentrated in individual aging super–star clusters that are themselves distributed throughout the nucleus. The *HST* images show other star clusters in the nucleus, and there must be still others which are optically obscured. If the starburst is made of a collection of super–star clusters, then the picture we have of starbursts is different from the one where starbursts are dominated by higher mass stars with a low-mass cutoff (Rieke et al. 1980, 1993). In particular, the IMF of a starburst may be more like that of globular clusters with a mass spectrum extending to well below a solar mass.

5. CONCLUSIONS

A three-component conceptual model for the starburst nucleus matches the three components of the nucleus identified by their different mid-IR and radio spectra. There is an AGN at the center of the galaxy that is responsible for the bright, nonthermal, radio point source as well as a volume of ionized gas with relatively little dissociated molecular material. The mid-IR and radio spectra indicate that most of the 6 cm radio from the center is nonthermal. Second, there is a young super–star cluster with several thousand O stars, H II regions, and photodissociation regions. In the cluster, most of the 6 cm radio emission is thermal, and there is significantly more mid-IR than predicted based on the flux of ionizing photons. Finally, there is a larger scale envelope with an older population of stars, star clusters, and supernovae remnants. In the envelope which may be energized by a population of older SSCs, about 30%–40% of the 6 cm radio emission is nonthermal. The difference between the one cluster which is much brighter in the mid-IR and the others in the envelope is that the mid-IR bright cluster may be much younger with most of its O stars still on the main sequence. The model of a starburst as a collection of superstar, proto–globular clusters predicts a starburst IMF with many low-mass stars, at odds with starburst models based on an IMF biased toward the high end of the stellar mass spectrum.

REFERENCES

Antonucci, R. R. J., & Ulvestad, J. S. 1988, ApJ, 330, L97
Barth, A. J., Ho, L. C., Filippenko, A. V., & Sargent, W. L. W. 1995, AJ, 110, 1009
Beck, S. C. & Beckwith, S. V. 1984, MNRAS, 207, 671
Benedict, G. F., et al. 1993, AJ, 105, 1369
Bower, G. A., & Wilson, A. S. 1995, ApJ, 99, 543
Carral, P., Hollenbach, D. J., Lord, D., Colgan, S. W. J., Haas, M. R., Rubin, R. H., & Erickson, E. F. 1994, ApJ, 423, 223
Cohen, M., Tielens, A. G. G. M., Bregman, J., Witteborn, F. C., Rank, D. M., Allamandola, L. J., Wooden, D., & de Muizon, M. 1989, ApJ, 341, 246
Cohen, M., Witteborn, F., Walker, R. G., Bregman, J. D., & Wooden, D. H. 1995, AJ, 110, 275
Conti, P. S., & Vacca, W. D. 1994, ApJ, 423, L97
Dudley, C. C., & Wynn-Williams, C. G. 1993, ApJ, 407, 65
———. 1997, ApJ, 488, 720
Forbes, D. A., Ward, M. J., & DePoy, D. L. 1991, ApJ, 380, L63
Genzel, R., Becklin, E., Wynn-Williams, C. G., Moran, J. M., Reid, M. J., Jaffe, D. T., & Downes, D. 1982, ApJ, 255, 527
Ho, L. C. 1996, in Rev. Mexicana Astron. Astrofis., Conf. Ser. 6, First Guillermo Haro Conf. Astrophys., Starburst Activity in Galaxies (City: Publisher), 5
Ho, L. C., & Filippenko, A. V. 1996a, ApJ, 466, 83
———. 1996b, ApJ, 472, 600
Ho, P. T. P., Beck, S. C., & Turner, J. L. 1990, ApJ, 349, 57
Ho, P. T. P., Turner, J. L., Fazio, G. G., & Willner, S. P. 1989, ApJ, 344, 135
Hoffmann, W. F., Fazio, G. G., Shivandan, K., Hora, J. L., & Deutsch, L. K. 1993, in Infrared Detectors and Instrumentation, ed. A. M. Fowler (Proc. SPIE, Vol. 1946), 449
Hoffmann, W. F., & Hora, J. L. 1997, MIRAC2 User's Manual, Version 6, 1997 September 11, (Steward Observatory, University of Arizona, and Harvard-Smithsonian Center for Astrophysics)
Hoffmann, W. F., Hora, J. L., Fazio, G. G., Deutsch, L. K., & Dayal, A. 1998, in Infrared Astronomical Instrumentation, ed. A. M. Fowler (Proc. SPIE, Vol. 3354), in press
Holtzmann, J. A., et al., 1992, AJ, 103, 691
Kalas, P., & Wynn-Williams, C. G. 1994, ApJ, 434, 546
Keto, E., Ball, R., Arens, J., Jernigan, G., Meixner, M., Skinner, C., & Graham, J. 1993, ApJ, 413, L23
Lacy, J. H., Beck, S. C., & Geballe, T. R. 1982, ApJ, 255, 510
Lebofsky, M. J., Montgomery, E. F., & Kailey, W. F. 1985 in Second NASA Ames Infrared Detector Technology Workshop, ed. C. R. McCreight (Mountain View: NASA), 14
Meurer, G. R., Hecjman, T. M., Leitherer, C., Kinney, A., Robert, C., & Garnett, D. R. 1995, AJ, 110, 2665
Mezger, P. G., & Henderson, A. P. 1967, ApJ, 147, 471
Moorwood, A. F. M., Lutz, D., Oliva, E., Marconi, A., Netzer, H., Genzel, R., Sturm, E., & de Graauw, Th. 1996, A&A, 315, L109
Mouri, H., Kawara, K., & Taniguchi, Y. 1997, ApJ, 484, 222
Paglione, T. A. D., Tosaki, T., & Jackson, J. M. 1995, ApJ, 454, L117
Paresce, F., De Marchi, G., & Romaniello, M. 1995, ApJ, 440, 216
Peng, R. Zhou, S., Whiteoak, J. B., Lo, K. Y., & Sutton, E. C. 1996, ApJ, 470, 821
Petrosian, V. 1970, ApJ, 159, 833
Petrosian, V., Silk, J., & Field, G. B. 1972, ApJ, 177, L69
Pina, R. K., Jones, B., Puetter, R. C., & Stein, W. A. 1992, ApJ, 401, L75
Puget, J. L., & Leger, A. 1989, ARA&A, 27, 161
Rieke, G. H., Lebofsky, M. J., Thompson, R. I., Low, F. J., & Tokunaga, A. T. 1980, ApJ, 238, 24
Rieke, G. H., Lebofsky, M. J., & Walker, C. E. 1988, ApJ, 325, 679
Rieke, G. H., Loken, K., Rieke, M. J., & Tamblyn, P. 1993, ApJ, 412, 99
Rieke, G. H., & Low, F. J. 1975, ApJ, 197, 17
Roche, P. F., Aitken, D. K., Smith, C. H., & Ward, M. J. 1991, MNRAS, 248, 606
Sams, B. J., Genzel, R., Eckarty, A., Tacconi-Garman, L. E., & Hofman, R. 1994, ApJ, 430, L33
Scoville, N. Z., Soifer, B. T., Neugebauer, G., Young, J. S., Matthews, K., & Yerka, J. 1985, ApJ, 289, 129
Shaya, E. J., Dowling, D. M., Currie, D. G., Faber, S. M., & Groth, E. J. 1994, AJ, 107, 1675
Spitzer, L. 1978, Physical Processes in the Interstellar Medium (New York: Wiley)
Turner, J. L., & Ho, P. T. P. 1985, ApJ, 299, L77
Ulvestad, J. S., & Antonucci, R. R. J. 1991, AJ, 102, 875
———. 1994, ApJ, 424, L29
———. 1997, ApJ, 488, 621
Watson, A. M., et al. 1996, AJ, 112, 534
Whitmore, B. C., & Schweizer, F. 1995, AJ, 109, 960
Whitmore, B. C., Schweizer, F., Leitherer, C., Borne, K., & Robert, C. 1993, AJ, 106, 1354
Wynn-Williams, C. G., Becklin, E. E., Matthews, K., & Neugebauer, G. 1979, MNRAS, 189, 163